Hybridized nearly-free-electron tight-binding-bond approach to interatomic forces in disordered transition-metal alloys. II. Modeling of metallic glasses

Ch. Hausleitner and J. Hafner
Institut für Theoretische Physik, Technische Universität Wien, Wiedner Hauptstrasse 8-10, A-1040 Wien, Austria
(Received 24 April 1991)

We present an atomistic simulation of the structure of transition-metal glasses based on interatomic forces derived from quantum theory. Using the inter-atomic potentials calculated within the hybridized nearly-free-electron tight-binding-bond theory introduced in the preceding paper, we construct models for Ni-Y, Ni-Zr, Ni-Nb, Ni-Ti, and Ni-V glasses using a molecular-dynamics quench. The results are in good agreement with the most accurate diffraction data. The analysis of the simulation data demonstrates a clear trend from trigonal-prismatic to polytetrahedral local order and from strong to moderate chemical order in the series Ni-Y, Ni-Zr, and Ni-Nb. Within a given system, the trend is from trigonal prismatic to polytetrahedral, and towards increasing chemical order with increasing Ni content. The correlation of the structural trend with the characteristic variation in the electronic structure is established.

I. INTRODUCTION

The atomic structure of amorphous metallic alloys has been a subject of intense research for many years.[1,2] Several distinct glass-forming alloy families have been established:[3–5] (a) the transition-metal–semimetal (or "metalloid") systems (e.g., Fe-B or Ni-P), (b) the intertransition-metal alloys (e.g., Ni-Zr or Fe-Ti), and (c) the simple-metal glasses (e.g., Mg-Zn or Ca-Al). For amorphous materials diffraction studies lead to a set of partial pair correlation functions, i.e., to a one-dimensional projection of a three-dimensional structure. Hence a fundamental understanding of the amorphous structure is possible only if the diffraction experiments can be supplemented with accurate modeling structures. For the simple-metal glasses of type (c) quite successful modeling studies using molecular-dynamics and potential-energy-mapping techniques[6,7] can be based on interatomic force fields derived from pseudopotential perturbation expansions.[8,9] Diffraction investigations and modeling studies show that the structure of most simple-metal glasses (Mg-Zn, Ca-Mg, Ca-Al, Mg-Ga,...) is rather well described in terms of polytetrahedral packing of atoms, modified by a certain degree of chemical short-range order, and by the necessity to accommodate atoms of different sizes.[10–12] However, for alloys with a very large size difference between the atoms such as Ca-Zn, computer simulations[13] predicted a pronounced topological short-range order which is best described as trigonal prismatic (distorted trigonal prisms of Ca, centered by Zn atoms), in analogy to the trigonal prismatic structures of the crystalline intermetallic compounds Ca_3Zn (Re_3B type), Ca_5Zn_3 (Cr_5B_3 type), and CaZn (CrB type). Later this prediction was confirmed by diffraction experiments.[14] Studies of the electronic properties[11,12,15] confirm and extend the results of the structural investigations, so that for simple-metal glasses today we have a detailed and realistic picture of the structural and electronic properties based on interatomic forces derived from quantum-mechanical concepts.

The situation is entirely different for the metallic glasses of types (a) and (b). For the metal-metalloid alloys the remarkable coincidence between the formation of glassy alloys and the formation of certain classes of crystalline intermetallic compounds has led to the development of stereochemically defined models. The crystalline borides, phosphides, silicides, etc., of those transition metals which readily form glasses with boron, phosphorus, and silicon have structures based on a trigonal-prismatic coordination of the metalloid by the transition-metal atoms. This characteristic local unit persists over a wide range of compositions and over a range of radius ratios differing widely from the ideal ratio for an undistorted trigonal prism. Thus this type of topology seems to be particularly stable. This has led to the proposal[15,16] that, in modeling the structure of the glassy phase, one should proceed by a random packing of these trigonal-prismatic units rather than of individual atoms. Later it was shown[17] that computer-generated models based on empirical pair forces can be made to possess a high degree of trigonal-prismatic order by adjusting the effective atomic size difference and the short-range metal-metalloid attraction.

For the intertransiton-metal glasses of type (b), attempts have been made to extend the application of the stereochemically defined models.[18,19] However this turns out to be rather difficult, because, unlike the metal-metalloid glasses, transition-metal glasses can be made over a very wide range of compositions and for systems with a strong (e.g., Ni-Y) to weak (e.g., Ni-Nb) chemical short-range order. Diffraction studies[20–23] indicate a

strongly varying degree of chemical as well as topological order, leading to a structure which is far more complex than that found in groups (a) or (c). Very recently[24,25] it has been shown that a reasonably accurate fit of the partial structure factors of Ni-Ti and Ni-Y glasses may be obtained using a model of nonadditive hard or soft spheres. It is quite surprising that introducing non-additivity [i.e., allowing for a distance of closest approach R_{12} for unlike spheres which deviates from the average diameter of the spheres, $R_{12} \neq (R_{11} + R_{22})/2$] alone allows for a description of the most salient features of *both* the topological and the chemical short-range order. However, it has to be noted that this approach treats the glass as a supercooled liquid and requires, beyond the fitting of the parameters of the model, the choice of a closure relation defining a set of integral equations for the pair correlation functions. Moreover, there is no possibility to relate the dominant nonadditivity parameter to realistic quantum mechanical bonding forces.

In the preceding paper[26] (hereafter referred to as I) we have presented a novel hybridized nearly-free-electron tight-binding-bond (NFE–TBB) approach to interatomic forces in disordered transition-metal alloys. This approach combines the conventional pseudopotential treatment of the *s*-electron contribution to the interatomic forces with a tight-binding-bond approach[27–29] to the pair forces mediated by the *d* electrons. In the simple, albeit realistic, approximation of nearest-neighbor *d*-*d* interactions and degeneracy of the five *d* bands the bond order relating the covalent bonding forces to the *d*-*d* transfer integral may be calculated analytically on a Bethe-lattice reference system. We have shown that the bond order depends strongly on the form of the *d* band in the alloy. As the electronic density of states changes from a common-band to a split-band form (e.g., in the series Ni-M, with M =Pd, Rh, . . . , or Zr, and Y or M =Co, . . . , or Ti), the pair forces in the alloy change from a set of additive pair potentials to nonadditive potentials with a strong preference for the formation of unlike-atom nearest-neighbor pairs and for bond distances in A–B pairs that are considerably shorter than in average A–A and B–B bond lengths. This means that the quantum-mechanically derived pair forces show all the distinctive features that have been found to be necessary for a realistic modeling of amorphous alloys.

In the second paper of this series we present a detailed investigation of the atomic structure of amorphous Ni-based alloys using molecular dynamics and the NFE–TBB pair forces. Ni-based metallic glasses have been selected for our study because only for the Ni alloys accurate partial correlation functions and structure factors are available from isotope-substitution experiments. A comparison of theory and experiment at the level of composite (neutron- or x-ray-weighted) structure factors only would not be a sufficiently stringent test of the theoretical predictions.

Given a set of interatomic potentials, the structural modeling proceeds by a simulated molecular-dynamics quench. Detailed results are presented for $Ni_{40}Ti_{60}$, $Ni_{58}V_{42}$, $Ni_{33}Y_{67}$, Ni_xZr_{1-x} (x = 0.35, 0.50, 0.65), and Ni_xNb_{1-x} (x = 0.44, 0.62). We find that the computer-generated models describe the complex structure of the amorphous transition-metal alloys very well. Most importantly, they describe the characteristic trends in a series such as Ni-Y, Ni-Zr, and Ni-Nb and as a function of composition, and allow to relate it to the changes in the electronic structure. On the basis of realistic three-dimensional models, we can proceed to an analysis of higher-order correlation functions. The investigation of the total and partial bond-angle-distribution functions is particulary fruitful. It is found that well-defined angular correlations exist in the glassy phase, that are very similar to those in the corresponding crystalline phases.

II. MOLECULAR DYNAMICS MODELING

We have performed microcanonical molecular-dynamics simulations of the liquid and glassy phases. For the integration of the Newtonian equations of motion we use a fourth-order predictor-corrector algorithm in the Nordsieck formulation,[30] with one iteration per corrector step. A "net-cube approximation to the cut-off sphere" (which is similar in spirit to the link-cell method[31]) is used for finding the atoms within the interaction radius around a given atom.[32,33] This technique has the advantage that at a fixed interaction radius both the computer time per integration step and the storage requirement grew only linearly with the total number of particles in the molecular dynamics cell.

Our simulations have been performed for $N = 1372$ atoms in the molecular dynamics cell, with a time increment of $\Delta t = 10^{-15}$ s. With this value of Δt, the total energy remains constant to within the four leading digits over several thousand integration steps. The interatomic potential is cut at a distance of about 25% of the cube edge of the molecular dynamics cell. With this cutoff, each interaction sphere contains about 100 atoms.

The simulation was started in the liquid phase. Typical runs took 4000–5000 steps for melting and equilibration and about as many for production. Pair correlation functions are based on averages of over 40 independent configurations taken at intervals of 100 time steps. For a production of the glassy phase the system is first compressed from the density of the melt to the higher density of the solid phase, at the same time the temperature was increased by 500 K to account for the higher melting temperature of the compressed phase and the system is reequilibrated. Alternatively, a new molecular dynamics run is started for the high-density–high-temperature melt. After equilibration, the results are perfectly undistinguishable. For the quench, the temperature is lowered quasicontinously in 8000 time steps to $T = 273$ K by scaling the velocities in intervals of 20 time steps. This corresponds to a quench rate of about $\dot{T} \simeq 10^{14}$ K s^{-1}. After quenching, the system is equilibrated for 2000 time steps, and finally 4000 time steps and 40 independent configurations are used for calculating pair correlation functions. Bond-angle distributions are calculated for only a small number of instantaneous configurations taken at larger time intervals.

For a comparison of the molecular dynamics quench

technique to other algorithms for modeling the structure of amorphous metals, we refer to the work of Grabow and Andersen.[34] We agree with the authors that the MD quenches lead to more realistic results than either cluster-relaxation or energy-minimization techniques, as they are not biased by the choice of starting configurations or cluster-building algorithms. The MD result depends on the interatomic potentials only.

III. NICKEL-BASED METALLIC GLASSES

In the following we shall describe the results for our MD simulations for Ni-based metallic glasses. The amorphous structures display a considerable degree of both topological and chemical order. We shall try to relate this short- and medium-range order to the structures of the crystalline intermetallic compounds. To prepare this discussion, it is convenient to recall very briefly the available information on the phase diagrams and structures of the crystalline intermetallic compounds.

A. Phase diagrams and crystal structures of alloys of Ni with 3*d* and 4*d* metals

Table I lists the most important intermetallic compounds formed by Ni with the early 3*d* and 4*d* transition metals from groups III to V (compiled after Pearson[35] and Villars[36]). There is a clear tendency to form tetrahedrally close-packed compounds (of a Frank-Kasper-type or based on the stacking of close-packed layers) in the Ni-rich regime of all alloys, and at intermediate concentration of the Ni-V and Ni-Nb alloys. Trigonal prismatic phases and structures based on the stacking of square-triangular nets of atoms are formed at smaller Ni concentrations in the Ni-Zr alloys. Thus there are two competing structural principles: polytetrahedral and trigonal-prismatic packing. These two structural principles are related to the glass-forming ability in a distinctly different way. This is illustrated very clearly in the Ni-Y phase diagram (see Hansen[37]): the Frank-Kasper phases ($Ni_{17}Y_2$, Ni_5Y, Ni_7Y_2, Ni_3Y, Ni_2Y) have high melting points, the trigonal-prismatic phases are located close to a deep eutectic minimum. The "easy" glass-forming region is centered around the eutectic. Note that in the Ca-Zn system which has a very similar phase diagram, the close relation between the formation of trigonal-prismatic phases and glass formation has been clearly established.[13,38] On the other end of the series, in the Ni-Nb and Ni-V systems we find only close-packed crystalline phases, and the glass forming includes the homogeneity range of a Frank-Kasper phase with a pronounced tendency to substitutional disorder (the μ-phase NiNb, and the σ-phase NiV.[39]

TABLE I. Crystal structures of intermetallic Ni-*M* compounds. Underlined: Structures built on the packing of triangular prisms or on the stacking of square-triangular nets. *Italics*: tetrahedrally close-packed structure (Frank-Kasper phases) and structures built on close-packed layers.

M =	Sc Y	Ti Zr	V Nb
NiM_3			Cr_3Si
NiM_2	Fe_3C $NiTi_3$	$NiTi_2$ Al_2Cu	*FeCr*
Ni_2M_3			
NiM	Ni_2Y_3 CsCl FeB	CsCl CrB	Fe_7W_6
Ni_2M	Cu_2Mg Cu_2Mg	Ni_2Ti Cu_2Mg	$MoPt_2$
Ni_3M	Be_3Nb	Ni_3Ti Ni_3Sn	Al_3Ti Al_3Ti/Cu_3Ti

B. Ni-Y glasses

We first present our results for amorphous Ni-Y alloys. This system is characterized by a very large radius ratio ($R_Y/R_{Ni} \sim 1.4$) and large differences in the number of *d* electrons and in the atomic *d*-electron eigenvalues. Therefore strongly nonadditive pair potentials and very strong ordering effects are expected. The pseudopotential- and tight-binding parameters for the calculation of the NFE-TBB pair interactions are given in Table I of I. The calculations have been performed for the experimental density, see Table II (for those alloys where no experimental data for the density are available, we calculate the density according to Vegard's law). The electronic density of states for the alloy $Ni_{33}Y_{67}$, calculated for a Bethe-lattice reference system, is close to the split-band limit, see Fig. 1(a). The lower part of the band is a nearly completely filled Ni band. The integration over the imaginary part of the off-diagonal Green's functions $G_{ij}(E)$ [Fig. 1(b)] leads to large differences to the bond orders Θ_{ij} (Table III) and to extremely nonadditive pair interactions $\Phi_{ij}(R)$ [Fig. 1(c)]. The repulsive diameters D_{ij} of the pair interactions (measured in terms of the position of the first node in the potential) are $D_{NiNi} = 2.8$ Å, $D_{NiY} = 2.4$ Å, and $D_{YY} = 3.6$ Å.

These values are very close to those obtained by Gazillo *et al.*[25] by fitting the partial structure factors of amorphous $Ni_{33}Y_{67}$ using a nonadditive hard-sphere reference system (note that no adjustable parameter enters in the calculation of the pair interactions of the alloy, all input

TABLE II. Input data for the molecular dynamics simulations: number density n (Å^{-3}) and temperature T_M (K) of the compressed melt before the quench.

Ni_xM_{1-x}	n (Å^{-3})	T_M (K)
$Ni_{33}Y_{67}$	0.0388	1923
$Ni_{35}Zr_{65}$	0.0527	1873
$Ni_{50}Zr_{50}$	0.0584	1973
$Ni_{65}Zr_{35}$	0.0655	1923
$Ni_{44}Nb_{56}$	0.0672	2073
$Ni_{62}Nb_{38}$	0.0734	2073
$Ni_{40}Ti_{60}$	0.0668	1973
$Ni_{58}V_{42}$	0.0823	2073

data being determined for the pure metals). In addition to the nonadditivity of the diameters, there is a strong attraction between Ni-Y pairs. The maximum depths of the potentials are $\varepsilon_{\mathrm{NiNi}} = -5$ mRy, $\varepsilon_{\mathrm{NiY}} = -41$ mRy, and $\varepsilon_{\mathrm{YY}} = -26$ mRy (cf. the bond orders given in Table III), hence the covalent bonding forces lead to a strong attraction between Ni and Y atoms.

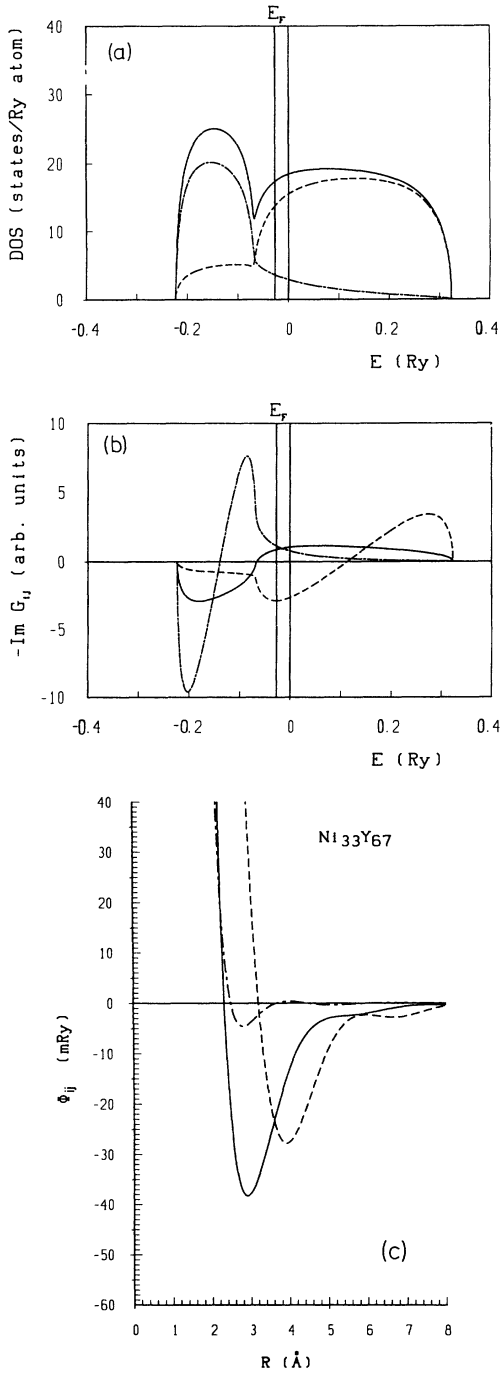

FIG. 1. (a) Total and site-decomposed electronic density of states for $Ni_{33}Y_{67}$, calculated for a random Bethe lattice. Solid line—total DOS, dashed line—partial Y DOS, dot-dashed line—partial Ni DOS. (b) Imaginary part of the off-diagonal Green's functions $\mathrm{Im}G_{ij}(E)$, dashed line—G_{YY}, dot-dashed line—G_{NiNi}, solid line—G_{NiY}. (c) Effective interatomic potentials $\Phi_{ij}(R)$. Same symbols as in part (b).

TABLE III. Bond orders Θ_{ij} for covalent d-d interactions in Ni-M alloys.

Alloy	$\Theta_{\mathrm{Ni\text{-}Ni}}$	$\Theta_{\mathrm{Ni}\text{-}M}$	$\Theta_{M\text{-}M}$
$Ni_{33}Y_{67}$	−0.604	−2.035	−1.385
$Ni_{35}Zr_{65}$	−0.591	−1.971	−2.110
$Ni_{50}Zr_{50}$	−0.666	−2.148	−2.123
$Ni_{65}Zr_{35}$	−0.794	−2.338	−2.048
$Ni_{44}Nb_{56}$	−0.613	−1.963	−2.662
$Ni_{62}Nb_{38}$	−0.724	−2.212	−2.783
$Ni_{40}Ti_{60}$	−0.732	−2.014	−2.154
$Ni_{58}V_{42}$	−0.751	−2.188	−2.639

The partial pair correlation functions $g_{ij}(R)$ and the static structure factors $S_{ij}(q)$ are in very good agreement with the experimental data of Maret *et al.*,[23] except for some smaller differences in g_{NiNi} at small Ni-Ni distances (Fig. 2). The Bhatia-Thornton structure factors show that the system is strongly chemically ordered, and there is also a high degree of topological order (the density-density structure factor $S_{\mathrm{NN}}(q)$ is quite different from that of a randomly close-packed system). The amplitude of the density-concentration structure factor $S_{Nc}(q)$ indicates a strong coupling between chemical and topological ordering. The Ashcroft-Langreth structure factors $S_{ij}(q)$ are strongly anomalous. In $S_{\mathrm{NiNi}}(q)$ the first peak at $q \sim 1.87$ Å^{-1} is a *prepeak* reflecting the chemical short-range order (CSRO), the peak related to the Ni-Ni nearest-neighbor distances is that close to $q = 2.6$ Å^{-1}. Note that there is no prepeak in the Y-Y structure factor. $S_{\mathrm{YY}}(q)$ is remarkable for the slowly decaying amplitude of the higher-order oscillation.

The largest difference between theory and experiment appears in the Ni-Ni structure factor and pair correlation function. Note, however, that our simulation results are considerably more realistic than either the nonadditive soft- and hard-sphere fits.[25] Both theory and experiment show the same characteristic three-peak structure in $g_{\mathrm{NiNi}}(R)$ at distances between $R = 2.5$ Å and $R = 6$ Å, albeit with some differences in position and amplitude. In making this comparison we should bear in mind that the correlation function for the minority species is the least accurately determined by experiment. At small distances the results are quite strongly influenced by termination errors. The unphysical values of the experimental $g_{\mathrm{NiNi}}(R)$ for $R < 2$ Å are an indication of these difficulties.

Given the pronounced structure in the correlation functions and the strong correlation between the glass-forming ability and the topology of the crystalline compounds, it is of course tempting to compare the crystalline and amorphous phases. The glass $Ni_{33}Y_{67}$ has no crystalline counterpart of identical composition. Crystallization leads to the formation of trigonal-prismatic compounds NiY_3 and Ni_2Y_3. In a trigonal-prismatic A_3B compound each A atom must belong on the average to two A_6B prisms. This can be achieved by sharing triangular faces (as in the Re_3B structure), or by sharing

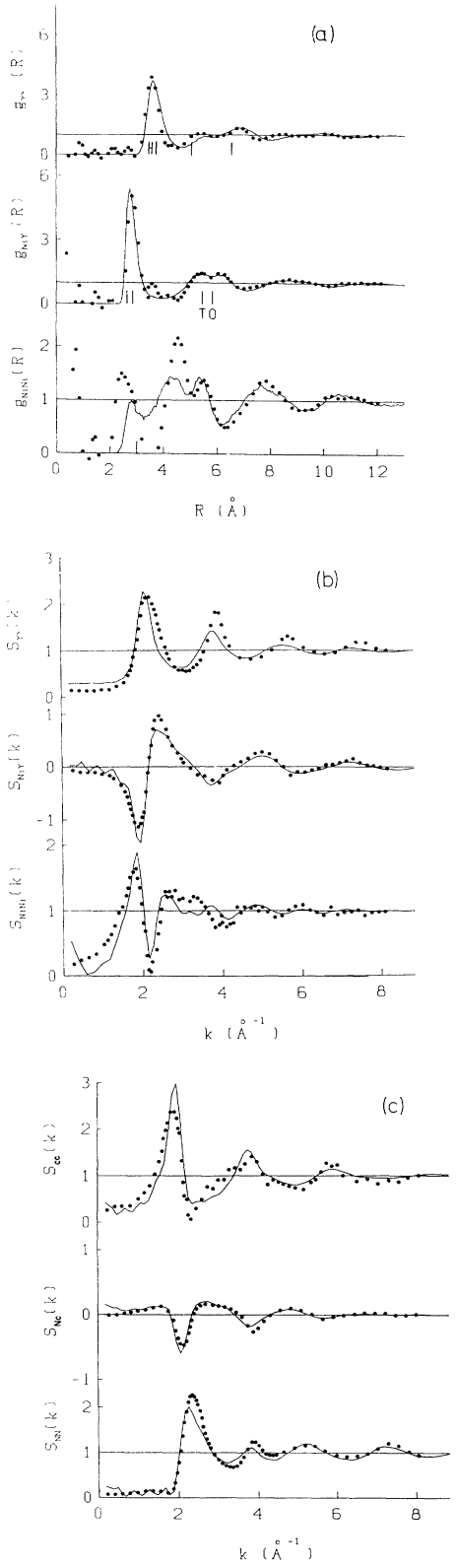

FIG. 2. Partial pair correlation functions $g_{ij}(R)$ (a), Ashcroft–Langreth (b), and Bhatia–Thornton (c) structure factors for amorphous $Ni_{33}Y_{67}$. Solid lines—molecular dynamics simulation, full dots—neutron-diffraction data (after Maret *et al.*, Ref. 23). The vertical bars in part (a) mark the interatomic distances in the crystalline structures (cf. text).

an edge with one and a vertex with a second prism (as in the Fe_3C and Ti_3P phases).[35] The shared vertex is also a capping atom for another prism, see Fig. 3(a). In the Ni_2Y_3 structure, each Y atom is shared on the average with two other prisms by forming four-prism clusters [Fig. 3(b)].

In the NiY_3 compound there are no direct Ni-Ni neighbors, in Ni_2Y_3 each Ni atom has on the average 1.5 Ni neighbors at a close distance of $d_{NiNi} = 2.52$ Å through face sharing. This coincides very well with the Ni-Ni nearest-neighbor distance in the amorphous phase, the Ni-Ni coordination number is 0.8. In both crystalline Ni-Y compounds there are well-defined Ni-Y distances of $d^{(1)}_{NiY} = 2.74$–2.90 Å corresponding to the center-to-vertex distance in the prisms, and Y-Y distances of $d^{(1)}_{YY} = 3.53$–3.61 Å corresponding to the height and base edges of the prisms and slightly larger distances of $d_{YY} = 3.8$ Å to Y atoms in adjacent prisms. Again there is a good correspondence between distances and coordination numbers in the crystalline and the amorphous phases [see Fig. 2(a) and Table IV].

The good correlation between the glassy and crystalline structures holds for the more distant neighbors. The second-neighbor Y-Y distance is given by the diagonal of the square face of the prism, $d^{(2)}_{Y\text{-}Y} = 5.1$ Å. In the Fe_3C- and Ti_3P-type arrangements, edge-sharing prisms are rotated by 215°, this leads to $d^{(3)}_{Y\text{-}Y} = 6.66$ Å. Both distances correlate quite well with the broad split second peak in $g_{YY}(R)$ [Fig. 3(a)]. Gaskell[16] has pointed out

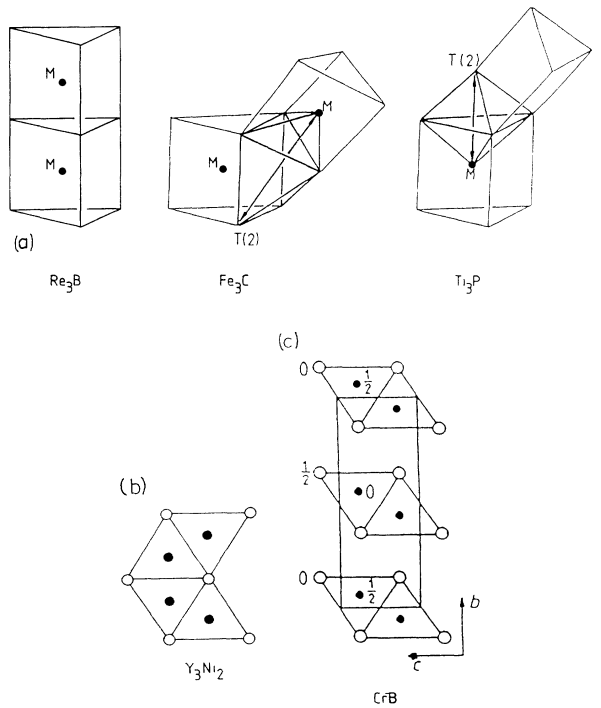

FIG. 3. (a) Connection of trigonal prisms in the Re_3B, Fe_3C, and Ti_3P structure. (b) Four-prism groups (projected as triangles) in the Ni_2Y_3 structure. (c) Layers of trigonal prisms (projected as triangles) in the CrB structure.

TABLE IV. Coordination numbers in amorphous $Ni_{33}Y_{67}$ and in the crystalline compounds NiY_3 and Ni_2Y_3.

	a-$Ni_{33}Y_{67}$	c-Ni_2Y_3	c-NiY_3
Ni-Ni	0.8	1.5	0.0
Ni-Y	7.2	8.0	6.0
Y-Ni	3.6	4.0	2.0
Y-Y	11.4	11.0	12.0

that it is possible to differentiate between the Fe_3C-type and Ti_3P-type arrangements through the distances from a metalloid to a second-neighbor metal atom $T(2)$ [see p. 42 of Ref. 16 and Fig. 3(a)]. In the former case the prisms are packed around a half-octahedron (O), in the latter case around a tetrahedron (T). With the radius ratio appropriate to Ni and Y ($R_{Ni}/R_Y = 0.77$ from the distances in the first peaks in g_{NiNi} and g_{YY}) one finds $d^{(2)}_{NiY}(T) = 5.56$ Å and $d^{(2)}_{NiY}(O) = 5.91$ Å. The correlation with the first part of the split second peak in g_{NiY} is slightly better for a Fe_3C- than for a Ti_3P-type arrangement. The correlation with the Ni_2Y_3-type structure is not so good. Sharing of square faces leads to a second-neighbor Y-Y distance of $d^{(2)}_{YY} \simeq \sqrt{3}\, d^{(1)}_{YY} \sim 6.25$ Å, and this falls rather in between the two maxima of the second peak in g_{YY}.

Thus the analysis of the pair correlation functions emphasizes the similarity of the amorphous Ni-Y structure with the cementite (Fe_3C)-type crystal structure and hence with Gaskell's stereochemically defined models for the metal-metalloid glasses. This correlation has already been pointed out by Steeb and Lamparter.[40] If the $g_{NiNi}(R)$ and the $g_{BB}(R)$ correlation functions of Ni-Y and Ni-B glasses, respectively, are plotted with the interatomic distances scaled by the shortest Ni-Y and Ni-B distances, there is a striking coincidence between the positions of the second and the third peaks in g_{NiNi} and the first two peaks in g_{BB} (see Fig. 4). This shows that transition-metal–metalloid (M-$\mathcal{M}$) and transition-metal-transition-metal (M-M) glasses have similar structures based on trigonal-prismatic packing. The difference is mainly in the degree of chemical order: in Ni-B there are no direct B-B neighbors at all, while in Ni-Y a small number of Ni-Ni contacts is allowed.

The topological short-range order is also evident from the distribution of the bond angles. In a tetrahedrally close-packed structure, the bond-angle distribution $f(\Theta)$ has two peaks at the icosahedral bond angles ($\Theta = 63.5°$ and $\Theta = 116.5°$),[41] and this distribution is only slightly changed if systems with larger size ratios are considered.[12] For the Ni-Y glass the total $f(\Theta)$ differs only slightly from this pattern, but characteristic differences are found in the partial bond-angle distributions (Fig. 5). The bonds centered at Y atoms form angles corresponding to those on the triangular and square faces of a distorted prism ($\Theta \sim 60°$, $\Theta \sim 90°$–$100°$) and to the rotation of two edge-sharing prisms ($\Theta \sim 145°$). The bond angles around the Ni atom in the glass correspond to the Y–Ni–Y bond angles within a slightly distorted tetrahedron ($\Theta \sim 75°$ and $\Theta \sim 135°$). There are only a few Ni-Ni-Ni triplets in the glass which form bond angles

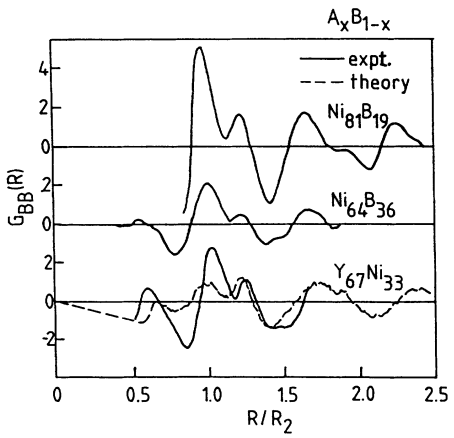

FIG. 4. Reduced pair correlation functions for the smaller atoms (B, respectively, Ni) in transition-metal–metalloid and Ni-M glasses. Distances are scaled relative to the shortest Ni-B and Ni-M distance, respectively.

centered around $\Theta \sim 110°$, i.e., close to the Ni–Ni–Ni angle in the four-prism group in the Ni_2Y_3 and also to the bond angles along the chains in a CrB structure where the trigonal prisms form layers.

The important point is that for the first time, a model of amorphous structure with trigonal-prismatic short- and medium-range order has been constructed on the basis of interatomic potentials derived from quantum theory, and with no adjustable parameters. The observed universality of the amorphous structure in M-$\mathcal{M}$ and M-M glasses is important for understanding why a model based on bond-order pair forces works so well. As angular forces derived from d-p or d-d interactions would be very different, it is unlikely that angular forces are im-

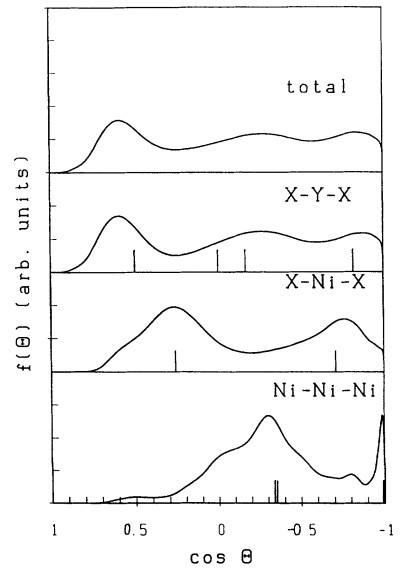

FIG. 5. Total and partial bond-angle distributions in amorphous $Ni_{33}Y_{67}$. All curves are normalized to the number of bonds.

portant for stabilizing the trigonal prisms. Rather, the local order is determined by the size ratio and, even more importantly, by the strong nonadditivity of the interatomic potentials. In that respect the analysis of Gaskell *et al.*[16,42] and of Gazillo *et al.*[25] supplement each other. They are very important for understanding the success of our NFE-TBB potentials.

C. Ni-Zr glasses

Ni_xZr_{1-x} glasses have been studied very intensively. Partial correlation function and structure factors are available for three different compositions: $x = 0.65$ (Ref. 22), $x = 0.50$ (Ref. 21), and $x = 0.35$ (Refs. 43 and 44). For all three metallic glasses, there exists a stable phase of nearly identical composition: Ni_2Zr (Cu_2Mg-type, cubic Laves phase), NiZr (CrB-type, trigonal prismatic), and $NiZr_2$ ($CuAl_2$-type). The interatomic potentials for this system have been discussed in detail in I. Compared to Ni-Y the nonadditivity is slightly reduced. The preferential Ni-Zr attraction is strongest in the Ni-rich alloy, otherwise the potentials are only weakly composition dependent.

For the $Ni_{35}Zr_{65}$ glass two independent determinations of partial correlation functions are available, one is based on neutron diffraction using isotopic substitution,[43] the second on x-ray diffraction and neutron diffraction, and a second x-ray experiment with partial "isomorphic" sub-

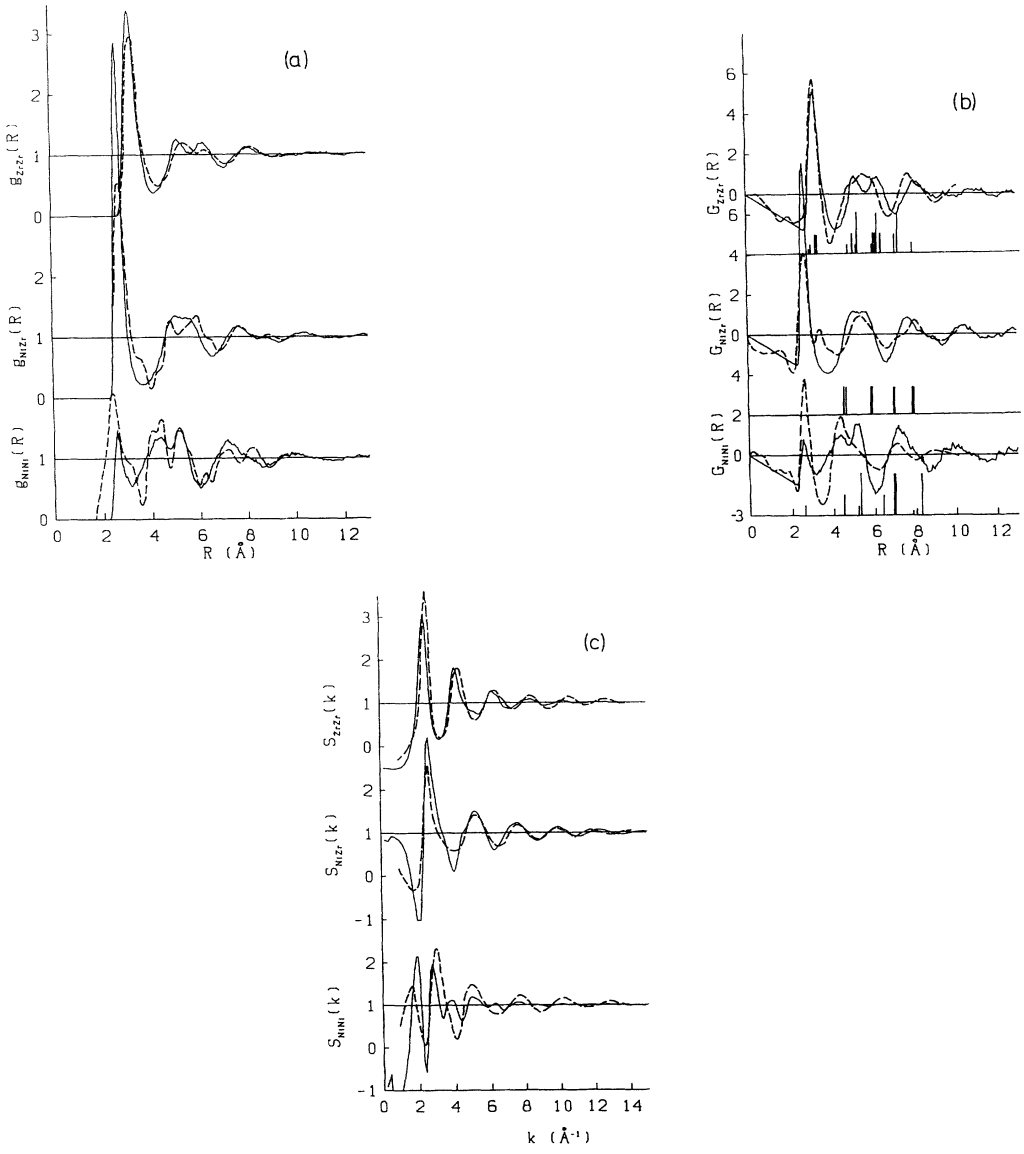

FIG. 6. (a) Partial pair correlation functions for the amorphous $Ni_{35}Zr_{65}$, as obtained by simulation and neutron diffraction (after Ref. 43). (b) and (c) Partial reduced pair distribution functions $G_{ij}(R)$ and structure factors $S_{ij}(q)$ for a-$Ni_{35}Zr_{65}$, compared with the isomorphic substitution experiment of Ref. 44. Solid lines—theory, dashed lines—experiment. The vertical bars represent the interatomic distances in the $CuAl_2$-type $NiZr_2$ compound, the height of each bar is proportional to the number of neighbors.

stitution of Zr by Hf.[44] The agreement between theory and experiment is distinctly better if we use the isotopic-substitution data (see Fig. 6), although the spikyness of the experimental data leads to the suspicion that the results are affected by termination errors. However, in the significant features of all three correlation functions, we find a full agreement between theory and experiment [Fig. 6(a)]. We also note the similarity with the correlation functions of amorphous $Ni_{33}Y_{67}$. These characteristic details do not appear in correlation functions of Wagner *et al.*,[44] which show a chemical ordering that is much weaker than in either the isotopic-substitution experiment of Mizoguchi *et al.*[43] or the simulation data [Figs. 7(b) and 7(c)]. $Ni_{35}Zr_{65}$ crystallizes in the $CuAl_2$ structure, and the peaks in the partial correlation functions show a reasonable correlation with the interatomic distances in the crystal. Combined with the analysis we presented in the last section, this should serve as a caveat: such corrrelations are important, but they should certainly not be overinterpreted.

For the $Ni_{50}Zr_{50}$ glass, simulation and experiment are in a nearly perfect agreement that extends to almost every detail of the correlation functions and structure factors (Fig. 7). The only difference is that the simulation results overestimate the degree of chemical order. This is reflected mainly in the relative amplitude of peak and prepeak in $S_{ZrZr}(q)$ [Fig. 7(b)]. We find a very remarkable coincidence between the peaks in the correlation functions and the interatomic distances in the CrB-type compound NiZr. In the CrB structure, the trigonal prisms form layers with the B(Ni) atoms centering the prisms arranged in zigzag chains. This feature is also reproduced by the bond-angle distributions (Fig. 8). On the whole, they are quite similar to the angular correlations in *a*-$Ni_{33}Y_{67}$ (Fig. 5), the distribution of the Ni–Ni–Ni bond angles show a pronounced peak at $\Theta \sim 110°$, i.e., very close to the chain angle of $\Theta = 112°$ in the CrB structure. In addition, there is a 60° peak indicating the presence of some tetrahedral complexes. The comparison of the coordination numbers (Table V) confirms the similarity of the crystalline and amorphous phase.

Given the good agreement between theory and experiment for the Zr-rich glasses, the mismatch observed between the calculated and experimental pair correlation functions and structure factors for $Ni_{65}Zr_{35}$ is somewhat disappointing (Fig. 9). Upon closer inspection however, we find that the reason for this discrepancy is almost entirely in one of the three diffraction experiments used for the calculation of the partials: the interference functions calculated for natural Ni and for the zero al-

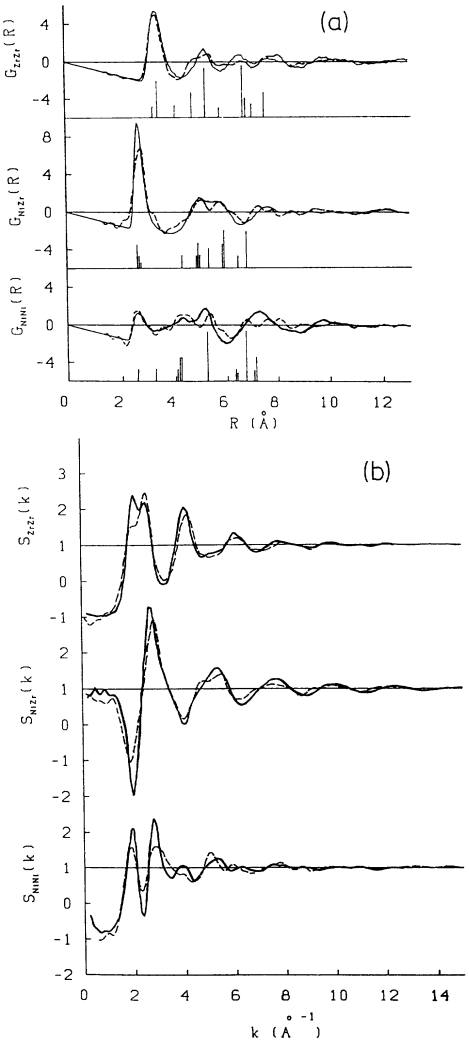

FIG. 7. Partial reduced radial distribution functions $G_{ij}(R)$ (a) and static structure factors $S_{ij}(q)$ (b) for amorphous $Ni_{50}Zr_{50}$. Solid lines—theory, dashed lines—neutron-diffraction (after Ref. 21). The vertical bars in (a) mark the interatomic distances in the CrB-type compound NiZr, the height of each is proportional to the number of neighbors.

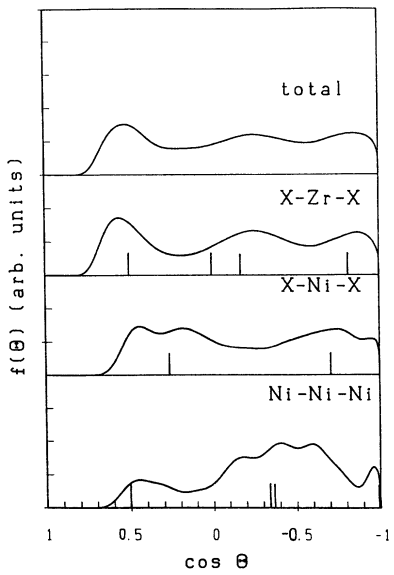

FIG. 8. Total and partial bond-angle distributions in amorphous $Ni_{50}Zr_{50}$. All curves are normalized to the numbers of bonds. Note that the peak in $f_{Ni\text{-}Ni\text{-}Ni}(\Theta)$ coincides with the angle in the Ni chains in the crystalline NiZr compound.

TABLE V. Interatomic distances and coordinations in Ni-Zr glasses and intermetallic compounds (cf. text).

		Glass				Crystal	
		d (Å)	N_{ij}	d (Å)	N_{ij}	d (Å)	N_{ij}
		Theory		Expt.[a]			
$Ni_{35}Zr_{65}$	Ni-Ni	2.60	1.2	2.45	3.3	2.63	2
($NiZr_2$)	Ni-Zr	2.70	8.2	2.85	8.6	2.76	8
	Zr-Ni	2.70	4.4	2.85	4.8	2.76	4
	Zr-Zr	3.25	10.7	3.30	11.0	2.99–3.43	11
$Ni_{50}Zr_{50}$	Ni-Ni	2.68	2.2	2.63	3.3	2.62	2
(NiZr)	Ni-Zr	2.75	6.1	2.73	6.7	2.68–2.78	7
	Zr-Zr	3.50	7.8	3.32	7.8	3.27–3.44	8
$Ni_{65}Zr_{35}$	Ni-Ni	2.55	5.6	2.52	6.0	2.45	6
(Ni_2Zr)	Ni-Zr	2.65	5.2	2.67	5.0	2.87	6
	Zr-Ni	2.65	9.6	2.67	8.8	2.87	12
	Zr-Zr	3.55	6.6	3.28	5.8	3.00	4

[a]After Ref. 43 ($Ni_{35}Zr_{65}$), Ref. 21 ($Ni_{50}Zr_{50}$), and Ref. 22 ($Ni_{65}Zr_{35}$).

loy agree well with experiment, whereas the interference function calculated for ^{60}Ni isotope shows pronounced differences (Fig. 10). Given the neutron-scattering length of $b(^{60}\text{Ni}) = 0.28$ and $b(\text{Zr}) = 0.71$ (Ref. 45), the weights for the Bhatia-Thornton structure factors in this experiment are $w_{NN} = 0.81$, $w_{Nc} = 1.62$, $w_{cc} = 0.81$. With these weighting factors, it is very surprising that the contribution from the first two peaks in $S_{cc}(q)$ (which is directly measured in the experiment with the zero alloy) should not appear more distinctly in the ^{60}Ni-interference function. This means that the experimental data should be interpreted with some caution. The published phase diagram for Ni-Zr shows no compound Ni_2Zr, but Villars and Calvert[36] list a cubic ($MgCu_2$-type) Laves phase Ni_2Zr. The correlation between the amorphous and crystalline phase is admittedly not quite as convincing as for

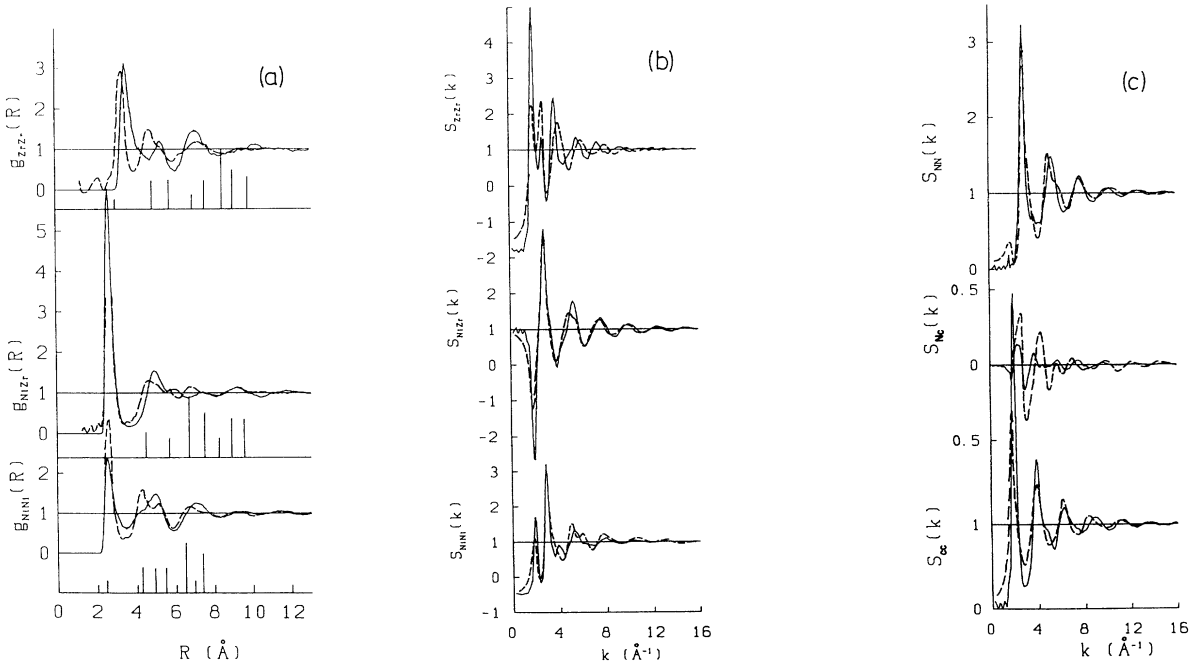

FIG. 9. Partial correlation functions $g_{ij}(R)$ (a), Faber-Ziman (b), and Bhatia-Thornton (c) structure factors for amorphous $Ni_{65}Zr_{35}$. Solid line—theory, broken line—experiment (after Ref. 22). The vertical bars mark the interatomic distances in the $MgCu_2$-type compound Ni_2Zr.

the more Zr-rich phases. The Laves phases are tetrahedrally close packed, and hence a strong similarity between the amorphous and crystalline phases of Ni_2Zr would imply a change in the short-range topology of the amorphous Ni-Zr phases as a function of composition. Significant changes are found in the Zr-Zr correlation function, the difference between $Ni_{65}Zr_{35}$ and $Ni_{50}Zr_{50}$ being much larger than between $Ni_{50}Zr_{50}$ and $Ni_{35}Zr_{65}$. g_{NiZr} is almost concentration independent. In g_{NiNi} there is a pronounced change in the amplitude of the first peak, and in the relative position of the second and third peaks (Fig. 11). In the angular correlations there is an appreciable change: the bond-angle distribution functions (Fig. 12) show that the surrounding of the Ni atoms is now essentially icosahedral, whereas the bond angles around the Zr atoms show a three-peaked distribution which correlates rather well with that in the larger 14-, 15-, and 16-fold coordination Frank-Kasper-polyhedra,[46,12] which

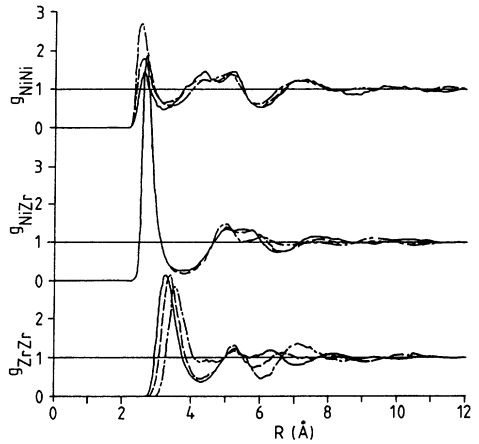

FIG. 11. Variations of the partial correlation functions $g_{ij}(R)$ in amorphous Ni-Zr alloys as a function of composition. Solid line—$Ni_{35}Zr_{65}$, dashed line—$Ni_{50}Zr_{50}$, dot-dashed line—$Ni_{65}Zr_{35}$.

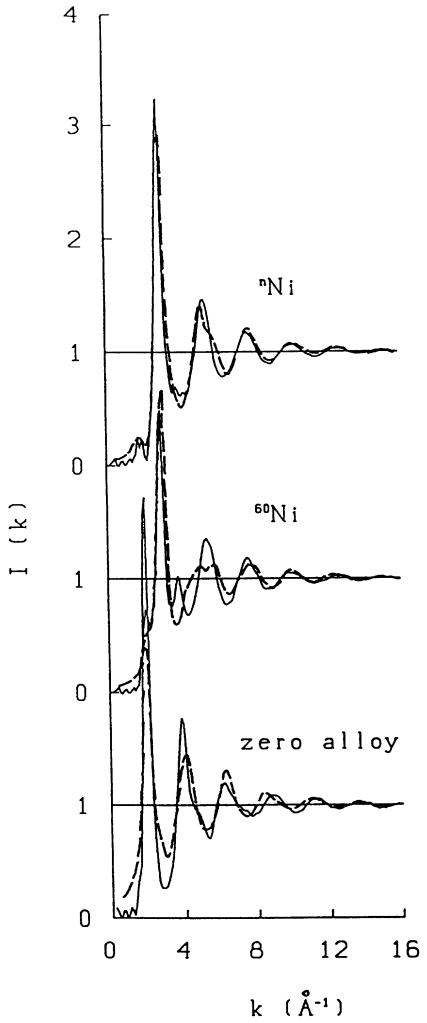

FIG. 10. Neutron-diffraction interference functions from amorphous $Ni_{65}Zr_{35}$ prepared with natural nickel, the ^{60}Ni isotope and from the zero alloy with isotope mixture $^{62}Ni_{0.615}{}^{60}Ni_{0.385}$. Solid line—theory, dashed line—experiment (after Ref. 22), see text.

are the coordination polyhedra of the larger minority atoms in the Frank-Kasper phases (only the polyhedron with 16 vertices is found in the Laves phase).

Altogether we are led to the conclusion that the short-range order is different in the Zr-rich and in the Ni-rich glasses: $Ni_{35}Zr_{65}$ and $Ni_{50}Zr_{50}$ have a trigonal-prismatic short-range order, while $Ni_{65}Zr_{35}$ is rather polytetrahedral. Some evidence that a change in the SRO occurs around the equiatomic composition has already been presented by Buschow.[47] He showed that the concentration dependence of the wave number Q_p of the principal peak in the x-ray interference function is linear over wide ranges of composition, but there is a distinct change of slope around 55% Ni. The point is that we have been able to show that these changes follow from a variation

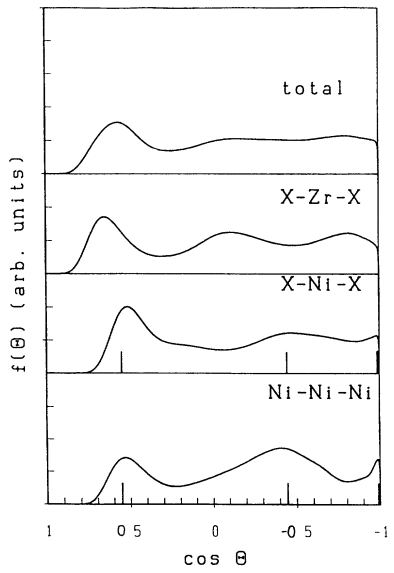

FIG. 12. Total and partial bond-angle distribution functions in amorphous $Ni_{65}Zr_{35}$ alloys.

of the pair interactions, i.e., mainly from the variation of the bond order induced by the change in the electronic density of states. (See I. Fig. 7 and Table III.)

D. Ni-Nb glasses

In I we have shown that with a decreasing difference in the number of d electrons of the components, the nonadditivity of the pair interactions decreases. The pair interactions for $Ni_{50}Nb_{50}$ is shown in Fig. 5(c) of I. Therefore we would expect a weaker CSRO and an amorphous structure which is closer to a polytetrahedral sphere packing. For Ni-Nb glasses, there have been various attempts to determine partial structure factors using anomalous x-ray diffraction[47] and using neutron diffraction and isotopic substitution.[48–51] Figures 13 and 14 show the partial reduced radial distribution functions for $Ni_{44}Nb_{56}$ and $Ni_{62}Nb_{38}$ glasses compared with the neutron-diffraction data.[49–51] The agreement between

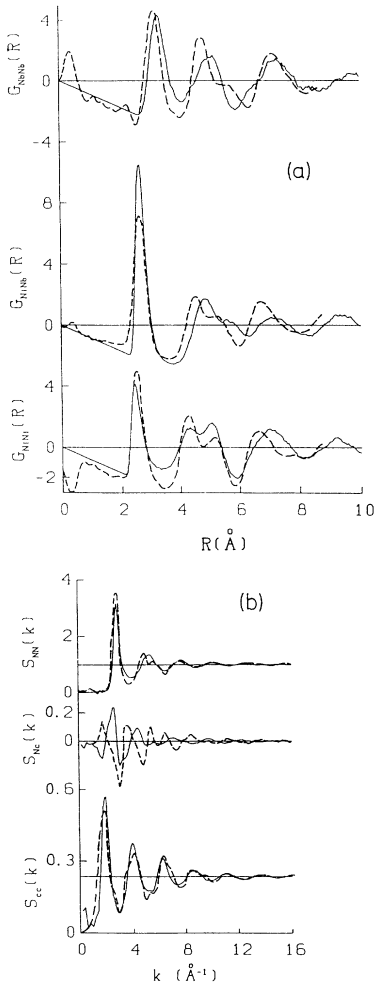

FIG. 13. Partial reduced radial distribution functions $G_{ij}(R)$ (a) and the Bhatia–Thornton structure factors for amorphous $Ni_{62}Nb_{38}$. Solid line—theory, dashed line—neutron diffraction (after Refs. 50 and 51).

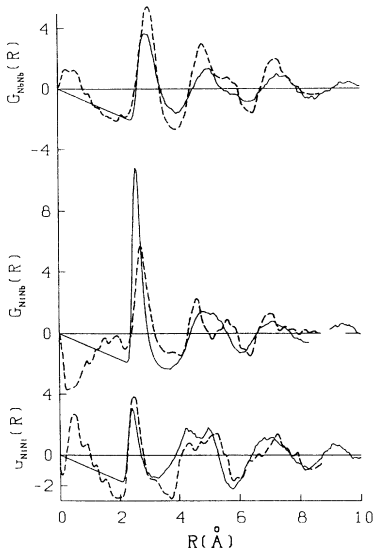

FIG. 14. Partial reduced radial distribution functions in amorphous $Ni_{44}Nb_{56}$. Solid line—theory, dashed line—neutron diffraction (after Ref. 51).

theory and experiment is only fair, but the oscillations at small distances indicate relatively large termination errors in the experimental results. We find that there is still an appreciable CSRO, but the overall arrangement of the atoms is now compatible with a polytetrahedral sphere packing (see Table VI). The CSRO is slightly stronger in the Ni-rich glass. There are only two crystalline phases in the Ni-Nb system. A tetrahedrally close-packed μ phase (Fe_7W_8-type) is formed in the composition range between 42 and 48 at. % Ni. The Ni_3Nb phase crystallizes

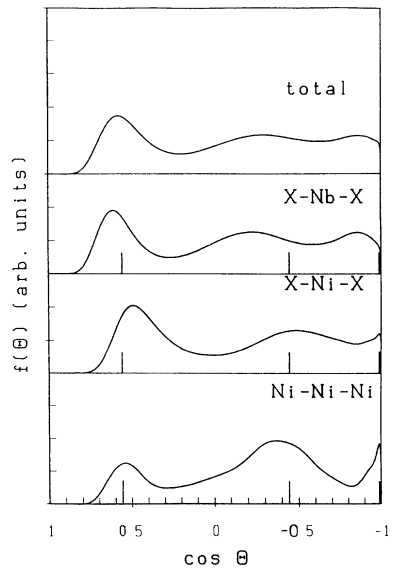

FIG. 15. Total and partial bond-angle distributions in amorphous $Ni_{44}Nb_{56}$. Vertical bars indicate the bond angle in an ideal icosahedron.

TABLE VI. Coordination numbers in amorphous $Ni_{44}Nb_{56}$ and $Ni_{62}Nb_{38}$, and in the μ-phase "NiNb."

	a-$Ni_{44}Nb_{56}$		μ-phase	a-$Ni_{62}Nb_{38}$	
	Theory	Expt.[a]		Theory	Expt.[a]
Ni-Ni	2.9	3.3	5.15	5.1	4.5
Ni-Nb	8.1	8.7	6.85	6.0	5.8
Nb-Ni	6.4	6.8	8.00	9.8	9.5
Nb-Nb	8.4	7.4	7.00	6.5	5.1

[a]After Ref. 51 ($Ni_{44}Nb_{56}$), and Ref. 50 ($Ni_{62}Nb_{38}$).

in the Cu_3Ti structure based on stacking of close-packed layers. In the μ phase, the larger atoms (Nb) are 12-, 14-, 15-, and 16-fold coordinated in the form of icosahedra and Frank-Kasper polyhedra, the smaller atoms (Ni) have an icosahedral surrounding. The bond-angle distributions (Fig. 15) and coordination numbers of the crystalline and amorphous phases indicate that in the glass we have again a dense, polytetrahedral packing.

Our results presented so far show that within the series of Ni-Y, Ni-Zr, and Ni-Nb amorphous alloys, the NFE-TBB pair forces predict a gradual change from a trigonal prismatic to a polytetrahedral topological short-range order and a decreasing chemical short-range order. We have also shown that as a function of composition, a transition from prismatic to tetrahedral is predicted with increasing Ni content. We now turn briefly to the metallic glasses of Ni with $3d$ metals.

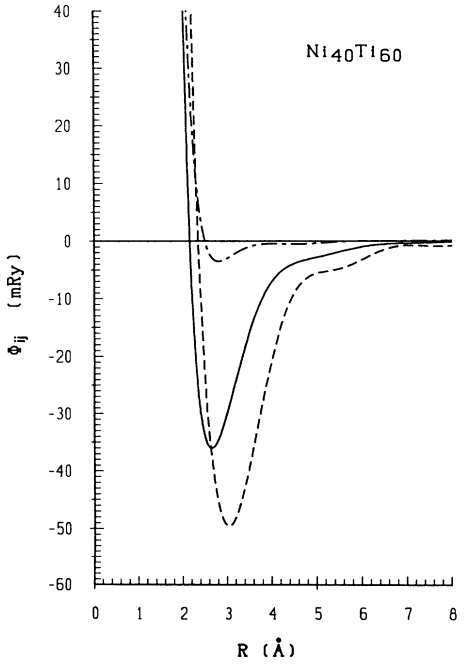

FIG. 16. Interatomic potentials $\Phi_{ij}(R)$ for $Ni_{40}Ti_{60}$. Dashed line—Φ_{TiTi}, solid line—Φ_{NiTi}, dot-dashed line—Φ_{NiNi}.

E. Ni-Ti glasses

The main difference between the pair interactions in Ni-Ti and Ni-Zr alloys arises from the smaller size and from the smaller bandwidth of the $3d$ metal Ti as com-

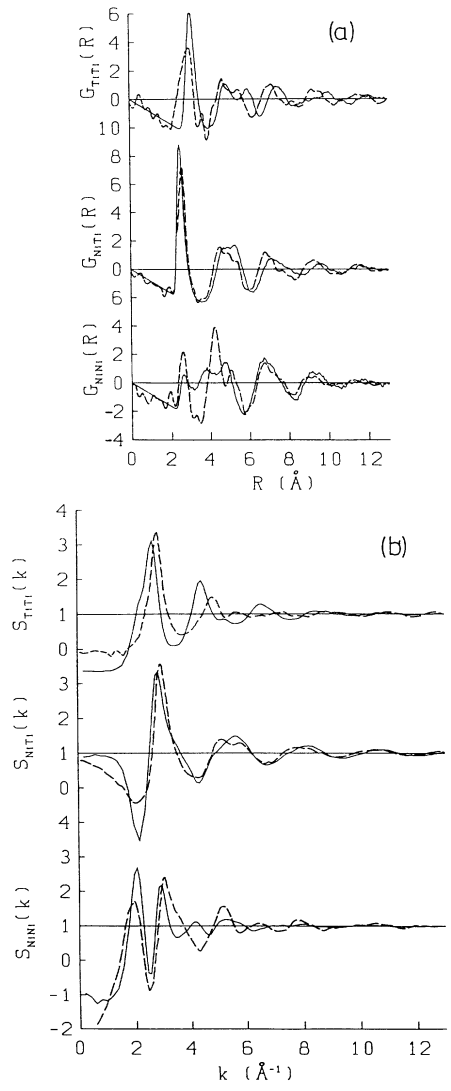

FIG. 17. Partial reduced radial distribution functions $G_{ij}(R)$ (a) and static structure factors $S_{ij}(q)$ (b) for amorphous $Ni_{40}Ti_{60}$. Solid line—theory, dashed line—experiment (after Ref. 20).

TABLE VII. Coordination numbers and interatomic distances in amorphous $Ni_{40}Ti_{60}$ and in the crystalline compound $NiTi_2$.

	Glass				Crystal	
	d (Å)	N_{ij}	d (Å)	N_{ij}	d (Å)	N_{ij}
	Theory		Expt.[a]			
Ni-Ni	2.63	1.8	2.63	2.3	2.87	3
Ni-Ti	2.50	8.1	2.60	7.9	2.49–2.89	9
Ti-Ni	2.50	5.4	2.60	5.3	2.49–2.89	6
Ti-Ti	3.06	9.5	3.01	8.1	2.91–2.99	9

[a] After Ref. 20.

pared to the $4d$ metal Zr. The nonadditivity of the Ni-Ti pair interactions is even more pronounced than in Ni-Zr: the Ni–Ti bond length is predicted to be smaller than either the Ni–Ni and the Ti–Ti bond lengths, the attractive part of the potential is strongest for Ni-Ti interactions (Fig. 16).

The partial reduced radial distribution functions and structure factors for $Ni_{40}Ti_{60}$ are shown in Fig. 17, together with the results of Fukunaga *et al.*[20] Inter-atomic distances and coordination numbers for the glass and for the crystalline compound $NiTi_2$ are given in Table VII. The agreement between theory and experiment is good for the Ni-Ti correlations, but only fair for Ni-Ni and Ti-Ti. Both the measured and calculated Ni-Ni distribution functions show the characteristic three-peak structure between $R = 2$ Å and $R = 6$ Å that we had found in Ni-Y and Ni-Zr glasses. However, whereas the calculated amplitudes are predicted to be quite similar in $Ni_{40}Ti_{60}$, $Ni_{50}Zr_{50}$, $Ni_{35}Zr_{65}$, and $Ni_{33}Y_{67}$, the experimental results show some distinct differences: For $Ni_{50}Zr_{50}$ and $Ni_{35}Zr_{65}$ the experimental results agree with the theoretical predictions, those for $Ni_{40}Ti_{60}$ and $Ni_{33}Y_{67}$ are different, but similar to each other. Note, however, that the difference is only in the amplitude of the peak, but not in their position. For distances larger than 6 Å however, both the calculated and the experimental correlation functions agree with those found in the Ni-Zr and Ni-Y systems. It is not clear as yet whether these differences are real and point to a difference in the local order of Ni-Zr glasses on one hand and Ni-Y and Ni-Ti glasses on the other hand. In any case, both theory and experi-

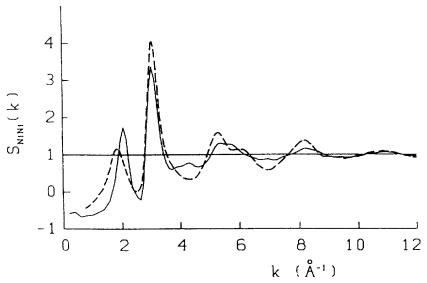

FIG. 18. Partial structure factor $S_{NiNi}(q)$ for amorphous $Ni_{58}V_{42}$. Solid line—theory, dashed line—experiment (after Refs. 52 and 53).

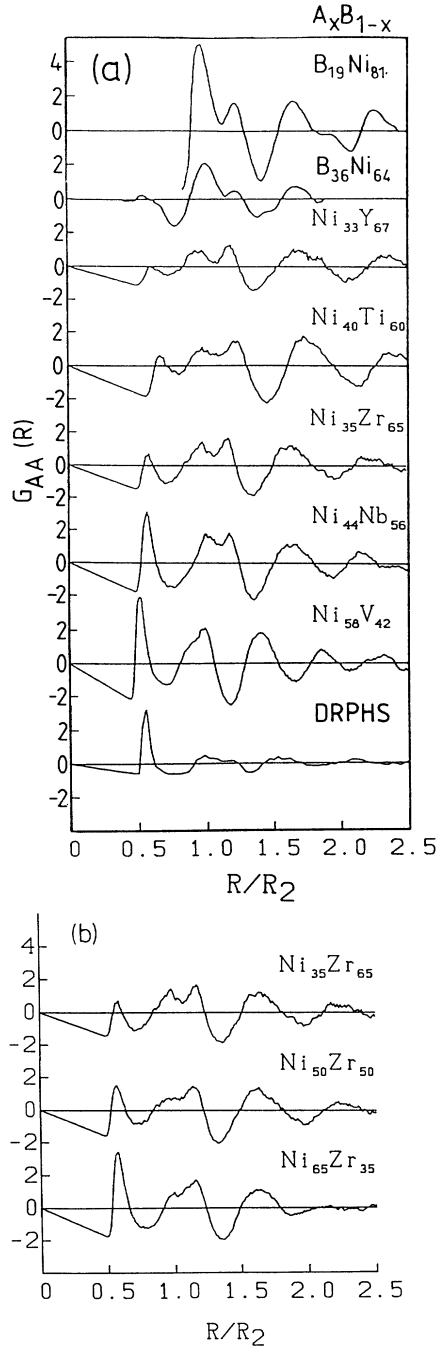

FIG. 19. (a) and (b) Ni-Ni and B-B correlation functions in Ni-B and Ni-M glasses. Distances are scaled to the position of the second peak (see text).

ment agree in that the local order increases on going from Ni-Zr to Ni-Y (i.e., to a system with a larger difference in the number of d electrons), and from Ni-Zr to Ni-Ti (i.e., from the $4d$ to the homologous $3d$ metal).

F. Ni-V glasses

We complete our investigation with a brief look at Ni-V glasses. No full set of partials is available, but because of the very small coherent scattering length of V ($b_V = -0.05$, $b_{Ni} = 1.03$), a neutron-diffraction experiment[52,53] measures directly the Ni-Ni partial structure factor. Again the computer simulation compares favorably with experiment (Fig. 18). Compared to Ni-Nb glasses of about the same composition we find a slightly increased chemical order. Compared to Ni-Ti glasses the local order is strongly reduced. Thus we find again the same trends in the local order as a function of group-number difference and on substitution of a $4d$ by a homologous $3d$ metal.

IV. CONCLUSIONS

We have presented an atomistic simulation of the structure of transition-metal glasses based on quantum-mechanically derived interatomic forces. We have shown that using our hybridized NFE-TBB pair interactions we are able to construct models in good agreement with the most accurate diffraction data. Moreover, the results of the simulations allow us to establish a clear trend from trigonal prismatic to polytetrahedral topological short-range order and from very strong to moderate chemical short-range order in the series Ni-Y, Ni-Zr, and Ni-Nb. With increasing Ni content within a given system the trend in the SRO is nuclear but the CSRO increases. This trend is expressed most clearly in the Ni-Ni correlation functions and Ni–Ni–Ni bond-angle distributions. In Ni-Y glasses the positions of the first three peaks in $g_{NiNi}(R)$ correspond almost exactly to the peaks in the B-B correlation function in $Ni_{64}B_{36}$ (Ref. 54) and $Ni_{81}B_{19}$ (Ref. 55), in the Ni-Nb glasses the form of $g_{NiNi}(R)$ is much closer to the dense-random-packing of hard spheres (DRPHS) limit [Fig. 19(a)]. The same transition from trigonal prismatic to random-close packed is observed in Ni_xZr_{1-x} glasses with increasing Ni concentration [Fig. 19(b)]. A corresponding trend is found in the Ni–Ni–Ni bond angles (Fig. 20). In Ni-Y and Ni-Ti glasses the bond angles are distributed around the chain angle of the Ni chains in the trigonal-prismatic (CrB-type) NiZr phase (similar bond angles are also found in Ni_2Y_3 and other trigonal-prismatic phases). In Ni-Zr and Ni-Nb glasses this distribution changes to one with three peaks at the bond angles in an icosahedron ($\Theta = 63.5°$, $\Theta = 116.5°$, and $\Theta = 180°$), emphasizing the same trend to a polytetrahedral local symmetry.

These changes may now be traced back to the variation of the interatomic forces and of the electronic structure. A pronounced nonadditivity of the pair interactions and a strong short-range interaction between unlike atoms lead to the formation of trigonal-prismatic clusters. As the nonadditivity is reduced, icosahedral clusters are preferred. In this respect we agree with the analysis of Fujiwara *et al.*[17] who showed that a strong, short-range M-M potential stabilizes trigonal-prismatic clusters over an octahedral arrangement, and also over an icosahedron at small radius ratios. The origin of the nonadditivity is in the strong covalent forces characteristic for alloys with a split-band density of states. Ongoing work in our group extends these investigations to Fe- and Co-based metallic glasses.

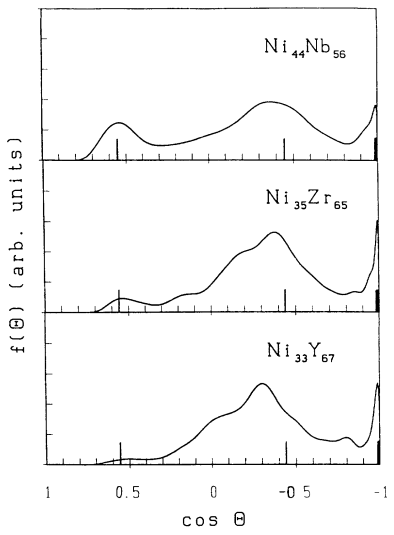

FIG. 20. Ni–Ni–Ni bond-angle distributions in Ni-M glasses. The bond angles in the Ni chains of the NiZr crystal and in a regular icosahedron are indicated.

The computer-generated structural models may serve as the basis for the calculation of the electronic structure, photoemission-, and x-ray spectra. Recent results on Ni_xZr_{1-x} glasses[56] show that very good agreement with experimental photoemission intensities can be achieved. As in the atomic structure, we find a strong correlation between the electronic density of states of the crystalline and amorphous phases. This supplements the arguments brought forward in the present paper.

Furthermore, the calculated density of states agrees reasonably with the Bethe-lattice model in the calculation of the interatomic forces. This would suggest that the interatomic forces, atomic, and electronic structures are consistent.

Note added in proof. Recently, our modeling studies have been extended to Fe- and Co-based metallic glasses.[57] Good agreement with diffraction data has been achieved. These structural models have been used in spin-polarized calculations of the electronic and magnetic structures. The results show that *ab initio* calculations of the magnetic phase diagram of amorphous alloys are now feasible.[58]

ACKNOWLEDGMENTS

This work was supported by the Bundesministerium für Wissenschaft und Forschung under Contract No. 49.658/3-II/A/4/90. We thank Professor V. A. Alekseev for communicating to us their a-NiNb data (Ref. 51) prior to publication.

[1] D. Turnbull and M. H. Cohen, J. Chem. Phys. **34**, 120 (1961).
[2] N. E. Cusack, *The Physics of Structurally Disordered Materials* (Hilger, Bristol, 1987).
[3] J. Hafner, in *Glassy Metals I*, edited by H. J. Güntherodt and H. Beck (Springer, Berlin, 1981), p. 93.
[4] S. R. Elliot, *Physics of Amorphous Materials* (Longmann, London, 1983).
[5] D.R. Nelson and I. Spaepen, in *Solid State Physics*, edited by H. Ehrenreich and D. Turnbull (Academic, New York, 1989), Vol. 39, p. 1.
[6] F. H. Stillinger and T. A. Weber, Phys. Rev. B **31**, 1954 (1985); **31**, 5262 (1985).
[7] J. Hafner, J. Phys. F **18**, 153 (1988).
[8] V. Heine and D. Weaire, in *Solid State Physics*, edited by H. Ehrenreich and D. Turnbull (Academic, New York, 1970), Vol. 24, p. 247.
[9] J. Hafner, *From Hamiltonians to Phase Diagrams* (Springer, Berlin, 1987).
[10] J. Hafner, S. S. Jaswal, M. Tegze, A. Pflugi, J. Krieg, P. Oelhafen, and H. J. Güntherodt, J. Phys. F **18**, 2583 (1988).
[11] S. S. Jaswal and J. Hafner, Phys. Rev. B **38**, 7311 (1988).
[12] J. Hafner and S. S. Jaswal, Phys. Rev. B **38**, 7320 (1988).
[13] J. Hafner and M. Tegze, J. Phys. Condens. Matter **1**, 8277 (1989).
[14] U. Mizutani, T. Shimizu, T. Fukunaga, T. Koyano, K. Tanaka, M. Yamada, and T. Matsuda, J. Phys. Condens. Matter **2**, 7825 (1990).
[15] P. H. Gaskell, in *Proceedings of the 3rd International Conference on Rapidly Quenched Metals*, edited by B. Cantor (Metals Society, London, 1978), Vol. 2, p. 277.
[16] P. H. Gaskell, in *Glassy Metals II*, edited by H. Beck and H. J. Güntherodt (Springer, Berlin, 1983), p. 5.
[17] T. Fujiwara, in *Topological Disorder in Condensed Matter*, edited by F. Yonezawa and T. Ninomiya (Springer, Berlin, 1983), p. 111.
[18] P. H. Gaskell, J. Non-Cryst. Solids **75**, 329 (1985).
[19] J. M. Dubois, J. Phys. (Paris) **46**, C8-335 (1985).
[20] T. Fukunaga, N. Watanabe, and K. Suzuki, J. Non-Cryst. Solids **61+62**, 343 (1984).
[21] T. Fukunaga, N. Hayashi, N. Watanabe, and K. Suzuki, in *Rapidly Quenched Metals*, edited by S. Steeb and H. Warlimont (Elsevier, New York, 1985), p. 475.
[22] S. Lefebvre, A. Quiry, J. Bigot, Y. Calvayrac, and R. Bellissent, J. Phys. F **15**, L99 (1985).
[23] M. Maret, P. Chieux, P. Hicter, M. Atzmon, and W. L. Johnson, in *Rapidly Quenched Metals* (Ref. 21), p. 521.
[24] D. Gazillo, G. Pastore, and S. Enzo, J. Phys. Condens. Matter **1**, 3469 (1989).
[25] D. Gazillo, G. Pastore, and R. Frattini, J. Phys. Condens. Matter **1**, 8463 (1990).
[26] Ch. Hausleitner and J. Hafner, preceding paper, Phys. Rev. B **45**, 128 (1992).
[27] A. P. Sutton, M. W. Finnis, D. G. Pettifor, and Y. Ohta, J. Phys. C **21**, 35 (1988).
[28] D. G. Pettifor, Phys. Rev. Lett. **63**, 2480 (1990).
[29] D. G. Pettifor, in *Many-Atom-Interactions in Solids*, edited by R. M. Nieminen, M. J. Puska, and M. J. Manninen (Springer, Berlin, 1990), p. 64.
[30] C. W. Gear, *Numerical Initial Value Problems in Ordinary Differential Equations* (Prentice Hall, Englewood Cliffs, New Jersey, 1966), Chaps. 9 and 10.
[31] D. Fincham and D. M. Heyes, in *Dynamical Processes in Condensed Matter*, edited by M. W. Evans (Wiley, New York, 1985), p. 493.
[32] A. Arnold, N. Mauser, and J. Hafner, J. Phys. Condens. Matter **1**, 965 (1989).
[33] A. Arnold and N. Mauser, Comput. Phys. Commun. **59**, 267 (1990).
[34] M. H. Grabow and H. C. Andersen, J. Non-Cryst. Solids **75**, 225 (1985).
[35] W. B. Pearson, *The Crystal Chemistry and Physics of Metals and Alloys* (Wiley, New York, 1972).
[36] P. Villars and L. D. Calvert, *Pearson's Handbook of Crystallographic Data for Intermetallic Phases* (American Society for Metals, Metals Park, Ohio, 1985), Vol. 1-3.
[37] M. Hansen, *Constitution of Binary Alloys* (McGraw-Hill, New York, 1958).
[38] M. Tegze and J. Hafner, J. Phys. Condens. Matter **1**, 8292 (1989).
[39] J. LeRoy, J. M. Moreau, D. Paccard, and E. Parthé, Acta Crystallogr. B **33**, 3406 (1977).
[40] S. Steeb and P. Lamparter, J. Phys. (Paris) **46**, C8-247 (1985).
[41] J. Hafner, J. Phys. (Paris) **46**, C9-69 (1985).
[42] J. M. Dubois, P. H. Gaskell, and G. Le Caër, in *Rapidly Quenched Metals*, edited by S. Steeb and H. Warlimont (Elsevier, New York, 1985), p. 567; P. H. Gaskell, *ibid.*, p. 413.
[43] T. Mizoguchi, S. Yoda, N. Akutsu, S. Yamada, J. Nishioka, T. Suemasa, and N. Watanabe, in *Rapidly Quenched Metals* (Ref. 41), p. 483.
[44] C. N. Wagner and D. Lee, J. Phys. (Paris) **41**, C8-242 (1980); A. Lee, G. Etherington, and C. N. J. Wagner, J. Non-Cryst. Solids **61+62**, 349 (1984).
[45] G. E. Bacon, Acta Crystallogr. A **28**, 357 (1972).
[46] F. C. Frank and J. S. Kasper, Acta Crystallogr. **11**, 184 (1958); **12**, 483 (1959).
[47] H. S. Chen and Y. Waseda, Phys. Status Solidi A **51**, 593 (1979).
[48] E. Svab, F. Forgacs, I. Hajdu, N. Kroo, and J. Takacs, J. Non-Cryst. Solids **46**, 125 (1981).
[49] E. Svab, L. Köszegi, G. Meszaros, and J. Takacs, Z. Phys. Chem. **157**, 5 (1988).
[50] E. Svab and S. N. Ishmaev, Exp. Techn. Phys. **36**, 89 (1988).
[51] V. A. Alekseev, S. N. Isakov, and S. N. Ishmaev (private communication).
[52] K. Suzuki, J. Non-Cryst. Solids **117+118**, 1 (1990).
[53] T. Fukunaga, Y. Homma, M. Misawa, and K. Suzuki, J. Non-Cryst. Solids **117+118**, 721 (1990).
[54] N. Cowlam, W. Gucan, P.P Gardner, and H. A. Davies, J. Non-Cryst. Solids **61+62**, 337 (1984).
[55] S. Steeb and P. Lamparter, J. Non-Cryst. Solids **61+62**, 237 (1984).
[56] W. Jank, Ch. Hausleitner, and J. Hafner, Europhys. Lett. **16**, 473 (1991).
[57] Ch. Hausleitner and J. Hafner (unpublished).
[58] I. Turek, J. Hafner, and Ch. Hausleitner (unpublished).